Published OnlineFirst June 3, 2021; DOI: 10.1158/0008-5472.CAN-20-4048

Upregulation of FGF9 in Lung Adenocarcinoma Transdifferentiation to Small Cell Lung Cancer

Kota Ishioka[1,2], Hiroyuki Yasuda[1], Junko Hamamoto[1], Hideki Terai[1,3], Katsura Emoto[4], Tae-Jung Kim[5], Shigemichi Hirose[6], Takashi Kamatani[1,7,8], Sachiyo Mimaki[9], Daisuke Arai[1], Keiko Ohgino[1], Tetsuo Tani[1], Keita Masuzawa[1], Tadashi Manabe[1], Taro Shinozaki[1], Akifumi Mitsuishi[1], Toshiki Ebisudani[1], Takahiro Fukushima[1], Mari Ozaki[1], Shinnosuke Ikemura[1,10], Ichiro Kawada[1], Katsuhiko Naoki[1,10,11], Morio Nakamura[2], Takashi Ohtsuka[12], Hisao Asamura[12], Katsuya Tsuchihara[9], Yuichiro Hayashi[4], Ahmed E. Hegab[1], Susumu S. Kobayashi[9,13], Takashi Kohno[14], Hideo Watanabe[15], David M. Ornitz[16], Tomoko Betsuyaku[1,†], Kenzo Soejima[1,3], and Koichi Fukunaga[1]

ABSTRACT

Transdifferentiation of lung adenocarcinoma to small cell lung cancer (SCLC) has been reported in a subset of lung cancer cases that bear EGFR mutations. Several studies have reported the prerequisite role of *TP53* and *RB1* alterations in transdifferentiation. However, the mechanism underlying transdifferentiation remains understudied, and definitive additional events, the third hit, for transdifferentiation have not yet been identified. In addition, no prospective experiments provide direct evidence for transdifferentiation. In this study, we show that FGF9 upregulation plays an essential role in transdifferentiation. An integrative omics analysis of paired tumor samples from a patient with transdifferentiated SCLC exhibited robust upregulation of FGF9. Furthermore, FGF9 upregulation was confirmed at the protein level in four of six (66.7%) paired samples. FGF9 induction transformed mouse lung adenocarcinoma-derived cells to SCLC-like tumors *in vivo* through cell autonomous activation of the FGFR pathway. *In vivo* treatment of transdifferentiated SCLC-like tumors with the pan-FGFR inhibitor AZD4547 inhibited growth. In addition, FGF9 induced neuroendocrine differentiation, a pathologic characteristic of SCLC, in established human lung adenocarcinoma cells. Thus, the findings provide direct evidence for FGF9-mediated SCLC transdifferentiation and propose the FGF9–FGFR axis as a therapeutic target for transdifferentiated SCLC.

Significance: This study demonstrates that FGF9 plays a role in the transdifferentiation of lung adenocarcinoma to small cell lung cancer.

Introduction

Lung adenocarcinoma and small cell lung cancer (SCLC) constitute distinct subgroups of human lung cancer (1). Cell of origins of lung adenocarcinoma and SCLC have been reported to be type II alveolar and neuroendocrine cells of the lung epithelium, respectively (2–5). However, the transdifferentiation of adenocarcinoma to SCLC has been frequently reported in clinical cases (6–12). Transdifferentiation between histological subtypes of cancer is usually a rare phenomenon, but has been reported in prostate cancer and lung cancer that have acquired resistance to molecular targeted therapeutics (6–9, 13–15), which suggests lineage plasticity of cancer cells. For example, the frequency of transdifferentiation of prostate adenocarcinoma to a more aggressive neuroendocrine prostate cancer has been reported to be 17% in 202 prostate cancer cases (16). Similarly, 5–15% of lung adenocarcinomas harboring activating epidermal growth factor receptor (*EGFR)* mutations transdifferentiate to SCLC after treatment with EGFR tyrosine kinase inhibitors (EGFR-TKI; refs. 7–9). Small cell transdifferentiation can also occur in anaplastic lymphoma kinase (ALK)-translocated non-SCLC (NSCLC) after ALK-TKI treatment (10), in NSCLC after immune-checkpoint inhibitor treatment (11) or in NSCLC without any treatment (12). These transdifferentiated cancers are no longer sensitive to either targeted therapy or immune-checkpoint inhibitor and show poor prognosis, which is in sharp

[1]Division of Pulmonary Medicine, Department of Medicine, Keio University, School of Medicine, Shinjuku-ku, Tokyo, Japan. [2]Department of Pulmonary Medicine, Tokyo Saiseikai Central Hospital, Minato-ku, Tokyo, Japan. [3]Clinical and Translational Research Center, Keio University School of Medicine, Shinjuku-ku, Tokyo, Japan. [4]Department of Pathology, Keio University School of Medicine, Tokyo, Japan. [5]Department of Hospital Pathology, Yeouido St. Mary Hospital, College of Medicine, The Catholic University of Korea, Seoul, South Korea. [6]Department of Pathology, Tokyo Saiseikai Central Hospital, Minato-ku, Tokyo, Tokyo, Japan. [7]Department of Medical Science Mathematics, Medical Research Institute, Tokyo Medical and Dental University, Tokyo, Japan. [8]Laboratory for Medical Science Mathematics, Department of Biological Sciences, Graduate School of Science, The University of Tokyo, Tokyo, Japan. [9]Division of Translational Genomics, Exploratory Oncology Research and Clinical Trial Center, National Cancer Center, Kashiwa, Japan. [10]Keio Cancer Center, School of Medicine, Keio University School of Medicine, Tokyo, Japan. [11]Department of Respiratory Medicine, Kitasato University School of Medicine, Japan. [12]Division of Thoracic Surgery, Department of Medicine, Keio University School of Medicine, Tokyo, Japan. [13]Department of Medicine, Beth Israel Deaconess Medical Center, Harvard Medical School, Boston, Massachusetts. [14]Division of Genome Biology, National Cancer Center Research Institute, Tokyo, Japan. [15]Department of Medicine, Division of Pulmonary, Critical Care and Sleep Medicine, Tisch Cancer Institute, Icahn School of Medicine at Mount Sinai, New York, New York. [16]Department of Developmental Biology, Washington University School of Medicine, St. Louis, Missouri.

Note: Supplementary data for this article are available at Cancer Research Online (http://cancerres.aacrjournals.org/).

K. Ishioka, J. Hamamoto, and H. Terai contributed equally to this article.

†Deceased.

Corresponding Author: Hiroyuki Yasuda, Division of Pulmonary Medicine, Department of Medicine, Keio University, School of Medicine, 35 Shinanomachi, Shinjuku-ku, Tokyo 160-8582, Japan. Phone: 81-3-3353-1211; E-mail: hiroyukiyasuda@a8.keio.jp

Cancer Res 2021;81:3916–29

doi: 10.1158/0008-5472.CAN-20-4048

Published OnlineFirst June 3, 2021; DOI: 10.1158/0008-5472.CAN-20-4048

contrast with the good prognosis of patients with NSCLC with effective targeted therapy (15, 17, 18). Several studies have reported that patients with transdifferentiated SCLC showed poorer prognosis than patients with *de novo* SCLC (12, 19). Therefore, to improve the prognosis of patients with lung cancer with transdifferentiated SCLC, understanding the mechanisms underlying transdifferentiation is essential.

Primary SCLC accounts for around 13% of lung cancer cases and is considered a deadly disease, with a 5.6% 5-year survival rate (20). SCLC is pathologically characterized by neuroendocrine features, and the expression levels of synaptophysin (SYP), chromogranin A (CHGA), calcitonin gene-related peptide (CGRP), neural cell adhesion molecule 1 (NCAM1, also known as CD56), and achaete-scute homolog 1 (ASCL1; refs. 21, 22) are used clinically or preclinically as markers of neuroendocrine differentiation. Recent genomic profiling of primary SCLC identified alterations in the retinoblastoma (*RB1*) and tumor protein 53 (*TP53*) genes (4, 5, 23), leading to simultaneous inactivation of these canonical tumor suppressors in almost all SCLC, indicating that these are prerequisites for SCLC development. Additional genetic alterations such as *MYC* amplification and inactivating mutations in epigenetic modifiers such as histone acetyl transferases, *CREBBP* and *EP300*, and NOTCH family members have also been reported (23–25). In addition, functional roles of several genes including *PTEN, RBL2, MYC*, and NOTCH pathway signaling genes (26, 27) in SCLC development have been reported in genetically engineered mouse models, indicating that these genetic and epigenetic alterations can be the "third hit" for SCLC development.

Several studies have determined some of the molecular characteristics of transdifferentiated SCLC (28–30). The genetic alterations of *TP53* and *RB1* genes have been repeatedly reported. A study has reported the inactivation of *RB1* in transdifferentiated SCLC, but it was not sufficient for the transdifferentiation to SCLC (28). Another report that evaluated the evolutional trajectories of SCLC transdifferentiation identified both *TP53* and *RB1* inactivation at an early stage of clonal evolution in transdifferentiation (30). The essential roles of the pathognomonic inactivation of *TP53* and *RB1* in transdifferentiation are consistent with primary SCLC, indicating that common pathway alterations exist between primary and transdifferentiated SCLC. However, inactivation of these canonical tumor suppressors is a prerequisite for transdifferentiation. Definitive additional events, the third hit, for transdifferentiation have not been identified. In addition, no prospective experiments have provided evidence of transdifferentiation. To understand the key biological processes in transdifferentiation, the identification of the third hit event and a prospective and functional evaluation are needed.

In this study, using paired samples from patients with lung cancer with confirmed transdifferentiated SCLC, we identified FGF9 upregulation as a key molecular event for SCLC transdifferentiation. Furthermore, we prospectively confirmed FGF9-mediated neuroendocrine differentiation in established mouse and human lung adenocarcinoma cells *in vitro* and *in vivo*, providing direct evidence for FGF9-mediated transdifferentiation.

Materials and Methods

Cell culture and stable cell lines

MLE12, H1975, H1650, H2228, H2087, H2110, A549, H441, H358, H69, H209, COR-L51, COR-L88, H82, and H146 were purchased from the ATCC and cultured in RPMI-1640 (Life Technologies) growth medium supplemented with 10% FBS and 1% penicillin/streptomycin. The BID007 cell line was established as described previously (31). To make stable cell lines that constitutively express FGF9, human *FGF9* and mouse *Fgf9* cDNA was amplified and cloned into the MigR1 retrovirus vector (#27490; Addgene). The MigR1 empty vector and MigR1-FGF9 vectors were transfected into Phoenix AMPHO or Bosc23 cells to make retrovirus particles. The medium containing the retroviruses was collected 48 and 72 hours after transfection. Infection was performed with polybrene. Of note, the MigR1 retrovirus vector contains an internal ribosome entry site (IRES)-eGFP sequence; highly positive GFP cells were, thus, sorted using flow cytometry (MoFlo XDP, ML99030; Beckman Coulter). The expression of *FGF9* in these cells was confirmed using quantitative RT-PCR and Western blotting. The stable cell lines that express EGFR that harbors activating mutations (L858R and an exon 19 deletion) were prepared as previously described (53). To create RB1-knockout cells, we used the RB1 CRISPR system (#KN206933; OriGene). gRNA vectors (scrambled or *RB1*) and donor DNA were transfected into target cell lines. Puromycin-resistant cells were selected as RB1-knockout cells, and a single clone was picked for each gRNA. The protein expression of RB1 in these cells was confirmed using Western blotting.

Reagents

AZD4547 (#S2801) was purchased from Selleck Chemicals. Recombinant FGF9 protein was purchased from Peprotech. Anti-phospho-p44/42 MAPK (Tyr202/Tyr204; #3126), anti-total p44/42 MAPK (#3127), anti-RB1 (#9309) anti-phospho-AKT (Ser473; D9E; #4060), and anti-total AKT (#9272) antibodies were purchased from Cell Signaling Technologies. An anti-actin antibody produced in mice (#A5441) and rabbit polyclonal antibodies against CGRP (#C8198) were purchased from Sigma-Aldrich. An anti-chromogranin antibody (#412751) and anti-synaptophysin antibody (#413831) were purchased from Nichirei Biosciences Inc. An anti-FGF9 antibody was purchased from R&D Systems (#AF-273NA) and Abcam (#ab71395). A goat anti-GFP polyclonal antibody (#600–101–215) was purchased from Rockland. A rabbit polyclonal antibody against FGFR1 (#sc-121) was purchased from Santa Cruz Biotechnology. Anti-EGFR (clone 3C6) and anti-Ki67 (clone 30–9) antibodies (CONFIRM kits) were obtained from Ventana-Roche.

Soft agarose gel colony formation assay

This assay was performed as described previously (32); we used 1×10^4 MLE12-FGF9 and MLE12-empty cells per well. After 4 weeks of culture, colonies were counted using a colony counter (Lumi vision analyzer; AISIN).

qRT-PCR

Total cellular RNA was isolated from cells using the RNeasy Mini Kit (#74106; Qiagen), and 2 μg of RNA was reverse-transcribed into cDNA using the High Capacity RNA-to-cDNA Kit (#4387406; Applied Biosystems). For qRT-PCR, we used an ABI Prism 7000 Sequence Detection System (Life Technologies). Relative quantification was performed using the ΔC_t method (cycle threshold), in which the ΔC_t value was calculated by subtracting the C_t value of each gene from that of human and mouse *GAPDH*. The data represent the average of three replicates from at least two independent experiments.

MTS cell proliferation assay

The MTS assay was performed as described previously (31). Briefly, H1975 cells (2×10^3 cells/well) were seeded into 96-well plates on day 1 and cultured for 72 hours. Subsequently, the relative cell numbers were measured. All conditions were tested in triplicate. The data represent

Published OnlineFirst June 3, 2021; DOI: 10.1158/0008-5472.CAN-20-4048

the average of three technical replicates; a representative experiment from at least two independent experiments is shown.

siRNA experiments

MLE12 cells were transfected with a final concentration of 20 nmol/L of siRNA targeting *FGFR1, FGFR2*, or *FGFR3* or of negative control siRNA (*FGFR1*: #s66023, #66024, *FGFR2*: #s201347, #s201348, *FGFR3*: #s66030, #s66031, Life Technologies). For transfection, SilentFect (#1703361; Bio-Rad) was used according to the manufacturer's protocol. Knockdown of the expression of *FGFR1, FGFR2*, and *FGFR3* was confirmed using qRT-PCR. SCLC cells were also transfected with siRNA targeting *FGF9* (#s230578, #s5146, #s5147) or negative control siRNA (#4390844; Thermo Fisher Scientific) at a final concentration of 20 nmol/L. Seventy-two hours after transfection, the relative number of viable cells was measured using the MTS cell proliferation assay.

Western blot analysis

Total proteins were extracted using cell lysis buffer (#9803; Cell Signaling Technologies). Protein concentrations were measured using the BCA protein assay (#23225; Thermo Fischer Scientific), and equal amounts of proteins were denatured and reduced using the sample buffer. After boiling the samples, their aliquots were subjected to SDS-PAGE. The fractionated proteins were transferred onto polyvinylidene difluoride membranes, which were then incubated first with primary antibodies, and then with secondary antibodies. For protein detection, the membranes were incubated with agitation in the LumiGLO reagent and peroxide (#7003S; Cell Signaling Technologies) and exposed to X-ray films.

Animal experiments and mouse xenograft model

All animal experiments were approved by the Laboratory Animal Center, Keio University School of Medicine. Female NOD/SCID and BALB/C nu/nu nude mice were purchased from Charles River. Mice were anesthetized with ketamine. H2228, H69, H209, COR-L88, and MLE12 cells transduced with or without *FGF9* were suspended in Matrigel (#356237; Corning) and were subcutaneously injected into the mice. Tumor volume was monitored using calipers. To evaluate drug efficiency, when the average tumor volume reached 100 to 200 mm^3, mice were randomized to receive either placebo (1% Tween 80, #T0546; Tokyo Chemical Industry Co.) or an FGFR inhibitor (AZD4547, 12.5 mg/kg) once a day via intragastric administration. Formalin-fixed and paraffin-embedded (FFPE) tissues from sacrificed animals were then subjected to IHC and immunofluorescence analysis. On the other hand, to examine tumor formation in the mouse lungs, MLE12-FGF9 cells were intravenously injected into the tail vein of NOD/SCID mice. Ten weeks after injection, tumor formation in the mouse lungs was confirmed using micro-CT (μCT). Subsequently, mice were sacrificed, and their lungs were harvested.

Immunofluorescence

Immunofluorescence was performed on cultured cells and paraffin-embedded sections from tumor-bearing mice as described previously (31).

IHC with human samples

IHC was performed, and slides were evaluated by expert pathologists from Keio University Hospital, Tokyo Saiseikai Central Hospital, and Yeouido St. Mary Hospital. FGF9 was stained as described previously (33). Of note, cell blocks of MLE12-empty and H1975 cell lines were used as negative controls, whereas those of MLE12-FGF9 and COR-L51 cell lines were used as positive-controls for FGF9 staining (Supplementary Fig. S1). The staining intensity in the cytoplasm was quantified based on an empirical 3-step scoring method (0, no staining; 1+, weak staining; 2+, strong staining); the samples with 1+ and 2+ staining intensity were defined as positive. Anti-EGFR and anti-Ki67 antibodies (prediluted) were also used on a Benchmark automated IHC platform (Ventana-Roche) using the CC1 m protocol and ultraView-HRP-based detection (34–36).

Gene expression analysis based on the Cancer Cell Line Encyclopedia database

Relative gene expression data for *FGF9*, other *FGF*s, and neuroendocrine markers were individually obtained from the Cancer Cell Line Encyclopedia (CCLE) database (https://portals.broadinstitute.org/ccle/; ref. 37). Fifty-three SCLC and 134 NSCLC cell lines were evaluated.

Gene expression analysis using the European Genome-Phenome Archive dataset

Gene expression data from 81 human SCLC samples (23) were used to obtain an expression heatmap and correlation matrix with pair-wise Pearson correlation coefficients, comparing the expression levels of *FGF9, FGF2, SFTPC*, and neuroendocrine marker genes within the dataset.

Whole-exome sequencing

Exome sequencing libraries using FFPE samples from case #1 were constructed following the manufacturer's protocol (SureSelectXT Human All Exome V6/V6 + UTRs Kit; Agilent). Using Trim Galore, we discarded short reads and reads with insufficient base qualities. The trimmed reads were aligned to the reference genome (GRCm38) using the Burrows–Wheeler Aligner (BWA); the index files required by BWA were generated separately. Several postprocessing steps were required to prepare the files for the detection of SNVs, loss of heterozygosity, and copy-number variations. CleanSam was used to obtain information on soft-clipped reads, which are only partially aligned to the reference genome. Next, these files were sorted using samtools. In addition, using Picard Readgroups, we marked reads that have been sequenced together. Then, duplicated reads (which were possibly PCR duplicates) were marked. Base recalibration was conducted in the final step of post-processing. Somatic point mutations and indels were called simultaneously, and the results were stored as a VCF file by running Mutect2 (tumor-only mode). Using FilterMutectCalls provided in the GATK package, probable technical or germline artifacts were removed. Using SelectVariants, all indels >10 bp were filtered out. Additional filters were used to decrease the false-positive rate of reported mutations; we applied filters for mutant allele frequency (≥10%) and coverage at particular positions in tumor samples (≥10×). To further reduce false-positive callings, the SNVs and indels were compared with different databases: CLINVAR (Benign/Likely_benign), Exome Aggregation Consortium and gnomAD (over 10% common SNP in East Asia), PolyPhen2 (score under 0.5), and SIFT (score over 0.05). All mutation information was visualized using mafrools (ver. 1.6.15). Of note, we tested whether two bam files were from the same patient using BamixChecker and calculated the genotype-concordance score (38). Mutation signature analysis was performed using SigProfiler (39).

Gene expression analysis

RNA was extracted from the FFPE samples (case #1). Using Trimomatic (ver. 0.38), we discarded short reads and reads with

Published OnlineFirst June 3, 2021; DOI: 10.1158/0008-5472.CAN-20-4048

insufficient base quality. The trimmed reads were then aligned with the reference genome (GRCm38) using STAR (ver. 2.7.0.f). TMM normalization and gene set enrichment analysis (GSEA) were performed using edgeR (ver. 3.22.3) and gprofiler2 (version 0.1.6), respectively.

Statistical analysis

Statistical analysis was performed using GraphPad Prism 5.0 (Graph Pad Prism Software Inc.). The Student *t* test was used for comparisons between two groups. For correlation studies, the Pearson correlation test was performed after the confirmation of parametric distribution. All *P* values were two-sided; *P* values <0.05 were regarded as statistically significant.

Data availability

The datasets generated during and/or analyzed in this study are available from the corresponding author upon reasonable request.

Study approval

This study was approved by the ethical review boards of Keio University School of Medicine (approval no. 20110171), Tachikawa Kyosai Hospital (approval no. 2016–06), Tokyo Saiseikai Central Hospital (approval no. 30–12), and St. Mary's Hospital (approval no. XC16SIMI0048S), and was performed in accordance with the Declaration of Helsinki. All human specimens were acquired from patients under the guidance of each institution. Written informed consent was obtained in all cases and all ethical regulations were followed. In addition, all animal experiments were approved by the Laboratory Animal Center, Keio University School of Medicine (approval no. 12115).

Results

FGF9 upregulation in a case of lung cancer with adenocarcinoma transdifferentiation to SCLC

First, we focused on a case (case #1) with confirmed adenocarcinoma to SCLC transdifferentiation. The patient was a 69-year old male with 40 pack-years of smoking history. This patient with lung adenocarcinoma harboring the *EGFR* L858R mutation was treated with gefitinib, a first-generation EGFR-TKI. After 24 months, when the patient experienced disease progression, a second biopsy revealed the L858R and T790M mutations. Therefore, osimertinib, a third-generation EGFR-TKI was administered. Five months after osimertinib treatment, the patient experienced disease progression and underwent a third biopsy (**Fig. 1A**). The third biopsy revealed transdifferentiation of the adenocarcinoma into SCLC with the *EGFR* L858R mutation. Fortunately, we were able to obtain paired samples, before and after EGFR-TKI treatment, and performed integrative molecular profiling, including whole-exome sequencing (WES) and RNA sequencing (RNA-seq). First, WES confirmed the identical patient origin of the paired samples (genotype-concordance score = 0.889). The original *EGFR* mutation L858R was confirmed in both pre- and postsamples, indicating that the *EGFR* mutation is a clonal event. The list of mutant genes is shown in Supplementary Fig. S2. A nonsense mutation in *RB1* was detected in the post-SCLC sample but not in the presample, and a missense mutation in *TP53* DNA binding domain was detected in the both samples (**Fig. 1B**). In addition, *PIK3CA* mutations and *MYC* amplification were not observed. Mutation signature analysis identified smoking-related signatures in both samples (Supplementary Table S1), reflecting the heavy smoking history of the patient. RNA-seq analysis revealed distinct expression profiles of the samples. The expression of neuroendocrine markers such as *NCAM1, CHGA, SYP, CHGB*, and *ASCL1* or small cell neuroendocrine signatures (SCN signatures; ref. 6) was upregulated in the transdifferentiated SCLC (**Fig. 1C**). Gene Ontology (GO) term analyses with upregulated/downregulated genes showed that 12 of the 40 pathways significantly altered by SCLC transformation were "neuron"-related terms (Supplementary Figs. S3A and S3B). Recently, primary SCLC has been classified into four groups depending on key transcriptomic patterns: ASCL1, NEUROD1, POU2F3, and YAP1 (40). In this case, the SCLC belonged to the ASCL1 type (**Fig. 1D**). The expression level of the *EGFR* gene was slightly lower in the post- than in the presample, which may reflect the loss of sensitivity to EGFR-TKIs. The expression levels of *TP53* and *RB1* were comparable (**Fig. 1E**). Interestingly, upregulation of the *FGF9* was observed in the post-SCLC sample (**Fig. 1E**). Of the upregulated genes, we focused on FGF9 because its overexpression has been associated with malignant phenotypes in multiple cancer cells (41–44), and FGF9-mediated neuroendocrine differentiation was observed in a mouse prostate cancer model (45). To confirm FGF9 upregulation at the protein level, we performed immunohistochemistry (**Fig. 1F**). Again, a robust upregulation of FGF9 was confirmed in the SCLC sample. In addition, to evaluate the specificity of *FGF9* upregulation in the context of transdifferentiation, the expression levels of other *FGF*s were also evaluated. A clear upregulation was observed only for *FGF9*, and not for other *FGF*s (**Fig. 1G**).

Upregulation of FGF9 in transdifferentiated SCLC cases

To confirm FGF9 upregulation in multiple cases of transdifferentiation to SCLC, we collected samples from multiple institutions in Japan and Korea. We obtained paired samples from five additional patients. The clinical characteristics or CT images of the patients are shown in Supplementary Table S2 and Supplementary Fig. S4, respectively. Although the *EGFR*-mutated NSCLC is associated with no or light smoking history (46), five of six cases (83.3%), including case #1, had dense smoking exposures. The mean smoking exposure was 44.1 pack-years in our cases, in clear contrast with the 3.1 pack-year history in a previous report (30). Notably, robust FGF9 upregulation was observed in four of six (66.7%) cases (**Fig. 2A** and **B**). Decreased expression of EGFR and increased expression of Ki67 were confirmed in cases #5 and #6; samples from the other cases were not available due to clinical reasons (Supplementary Fig. S5; Supplementary Table S3). Increased expression of FGFR1 was observed in case #6 (Supplementary Fig. S5). Altogether, these data indicate that the upregulation of FGF9 is a common event in adenocarcinoma to SCLC transdifferentiation, although the functional roles of FGF9 in transdifferentiation still remain elusive.

To seek the clinical relevance of FGF9 expression in the transdifferentiated SCLC, we evaluated FGF9 expression in primary SCLC because primary and transdifferentiated SCLC share common molecular alterations in the oncogenic process. Interestingly, the *FGF9* expression level was positively correlated with the expression of neuroendocrine markers such as *ASCL1, CHGA*, and *NCAM1* in previously reported human primary SCLC dataset (**Fig. 3A** and **B**; ref. 23). In a cancer cell line dataset (37), *FGF9* mRNA expression level was significantly higher in SCLC than in NSCLC cells (**Fig. 3C**; Supplementary Fig. S6), and it was positively correlated with neuroendocrine marker genes (**Fig. 3D**; Supplementary Fig. S7A and B). Interestingly, the knockdown of *FGF9* or the inactivation of the FGFR pathway inhibited the growth of an FGF9-expressing SCLC cell line, H69 cells, *in vitro* and *in vivo* (Supplementary Figs. S8A–S8C), although no functional roles of

Published OnlineFirst June 3, 2021; DOI: 10.1158/0008-5472.CAN-20-4048

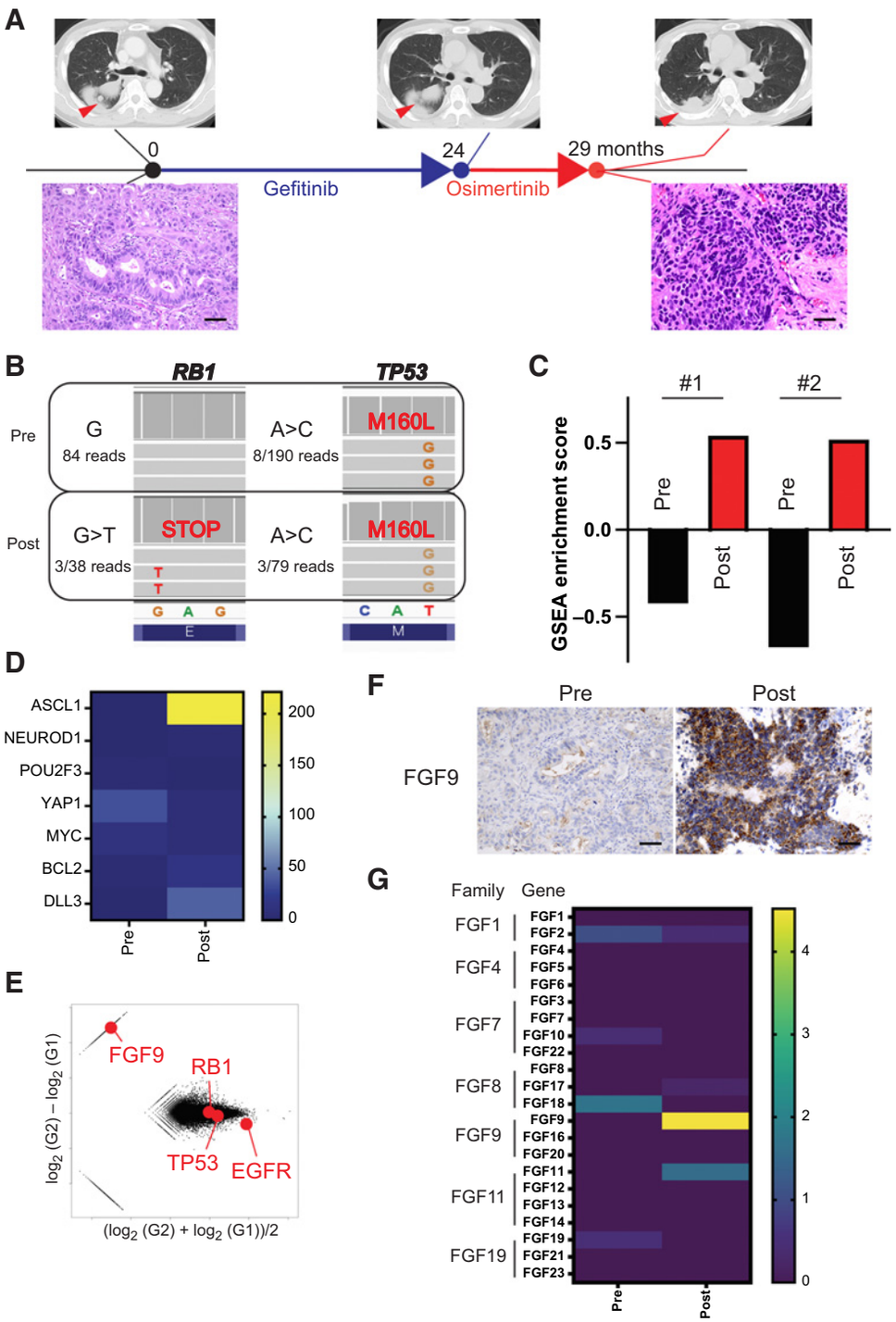

Figure 1.

Comparisons of genomic and mRNA expression data between adenocarcinoma (pre) and small cell lung cancer (post) in an FFPE sample derived from one transdifferentiated patient. **A,** Treatment history. Arrowheads in computed tomography images indicate tumors. Representative images of hematoxylin and eosin (H&E) staining. Scale bars, 200 μm. **B,** E492* mutation of *RB1* in small cell lung cancer (post), and M160 L mutation of *TP53* in adenocarcinoma (pre) and small cell lung cancer (post). **C,** GSEA score of neuroendocrine markers. *NCAM1, CHGA, SYP, CHGB, INSM1, ASCL1, GRP, SCG2, UCHL1, CALCA, CALCB*, and *NEUROD1* were used in #1; 33 genes listed as pan-cancer SCN signatures (6) were used in #2. **D,** mRNA levels of SCLC subtype markers. **E,** mRNA levels of *FGF9, TP53, RB1*, and *EGFR*. **F,** Expression of FGF9 as detected by IHC in sections of the first and second biopsy samples. Scale bars, 200 μm. **G,** mRNA levels of *FGF* family genes.

Published OnlineFirst June 3, 2021; DOI: 10.1158/0008-5472.CAN-20-4048

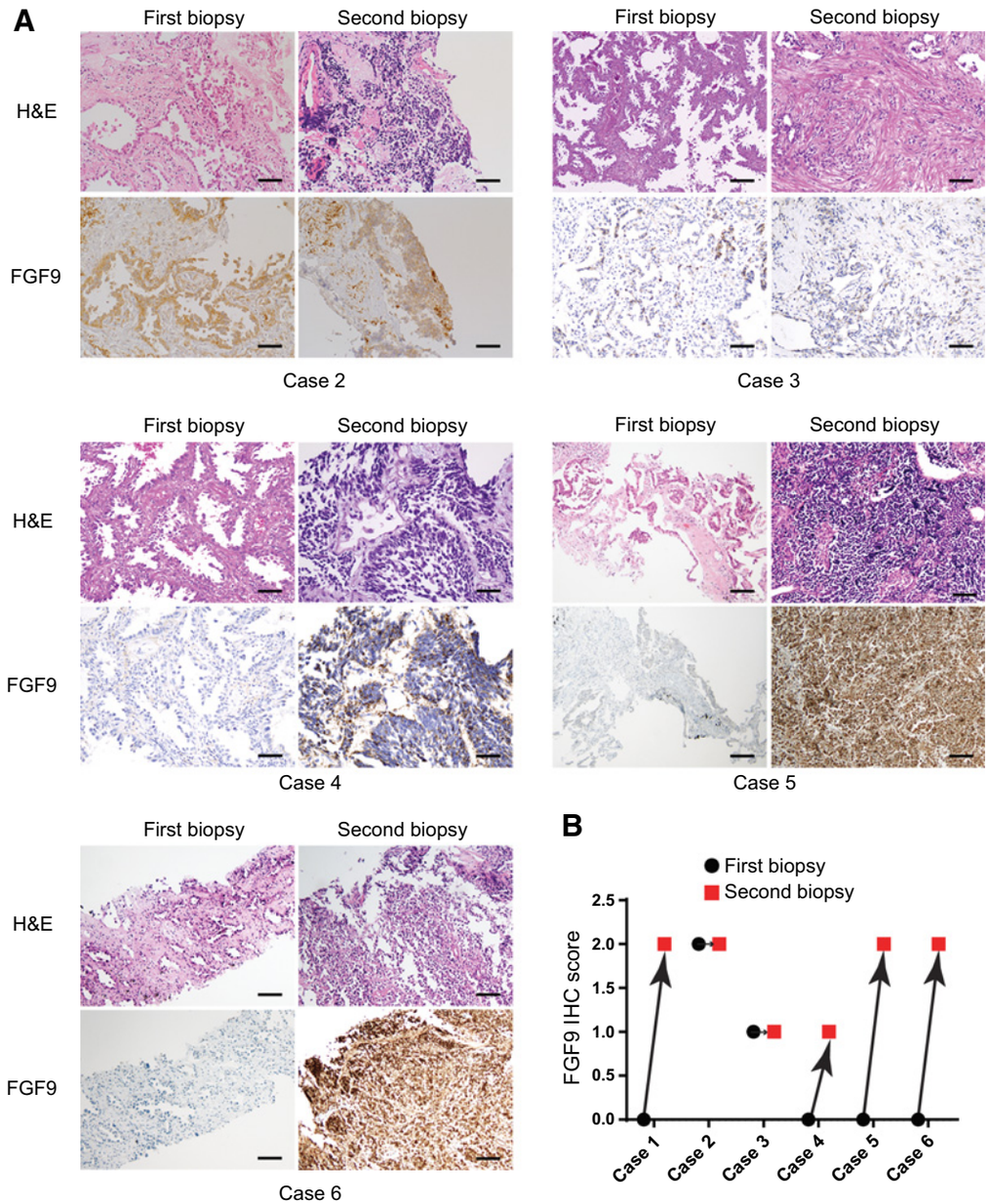

Figure 2.

Clinical evidence for FGF9 upregulation in the transdifferentiated SCLC. **A,** Representative images of hematoxylin and eosin (H&E) staining and the expression of FGF9 by IHC in sections of first and second biopsies of cases 2 to 6. Scale bars, 200 μm. **B,** FGF9 IHC scores of first and second biopsy samples

FGF9 were observed in other FGF9-expressing SCLC cell lines. Therefore, these data suggest that FGF9 plays a functional role in a subgroup of primary SCLC.

In fact, the expression of FGF9 was confirmed in 45 of 69 (65.2%) of our original SCLC samples (**Fig. 3E** and **F**; Supplementary Table S4). FGF9 is reported to be expressed in epithelial and mesothelial cells of embryonic lungs and downregulated in normal adult lungs (47). Consistent with this report, FGF9 expression was not observed in adjacent noncancer tissues. These data support the clinical relevance of FGF9 upregulation in transdifferentiation.

FGF9 transforms mouse lung adenocarcinoma-derived cells to SCLC

Our observation that FGF9 is upregulated in multiple cases of transdifferentiation and that FGF9 expression is positively associated with neuroendocrine marker gene expression prompted us to prospectively evaluate the functional roles of FGF9 in transdifferentiation.

First, we introduced *FGF9* into MLE12 cells (Supplementary Fig. S8). MLE12 cells, which express the large T antigen that inactivates *Tp53* and *Rb1*, are mouse lung epithelial cells derived from mouse lung adenocarcinoma (32, 48). FGF9 induction significantly increased 3D

Published OnlineFirst June 3, 2021; DOI: 10.1158/0008-5472.CAN-20-4048

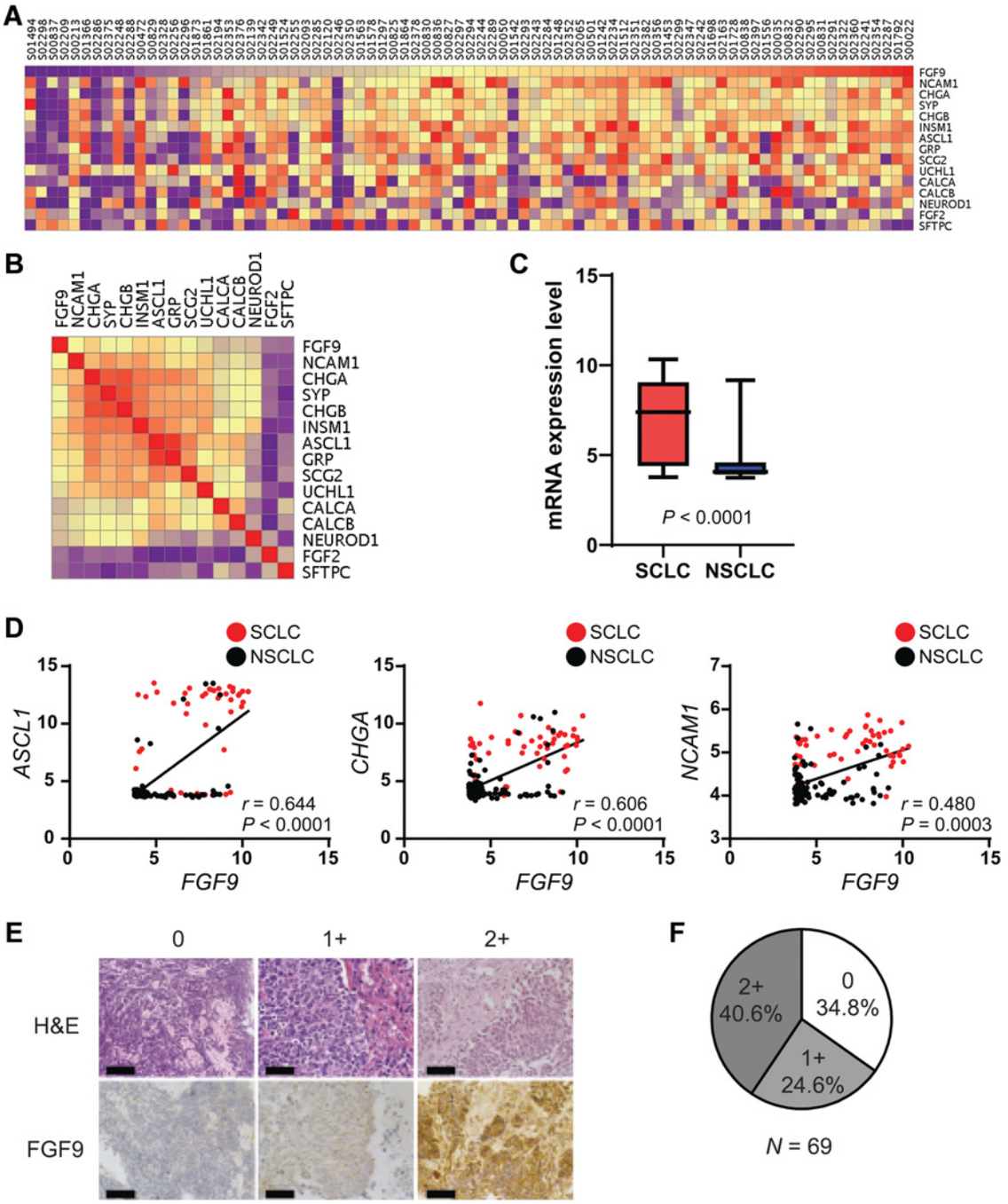

Figure 3.

Association between FGF9 expression and neuroendocrine differentiation in primary SCLC. **A,** Heatmap depicting the relative mRNA levels of *FGF9, FGF2*, neuroendocrine markers, and other lineage marker genes in a human SCLC dataset. **B,** Pearson correlation matrix of *FGF9, FGF2*, and neuroendocrine marker genes. Positive correlations are shown in red, and negative correlations are shown in blue. **C,** *FGF9* mRNA expression level in human SCLC ($n = 53$) and NSCLC ($n = 134$) cell lines. **D,** Scatter plots for the expression of *FGF9* and neuroendocrine marker genes, *ASCL1, CHGA*, and *NCAM1* in human SCLC ($n = 53$) and NSCLC ($n = 134$) cell lines. *r* indicates Pearson correlation. **E,** Representative images of hematoxylin and eosin (H&E) staining and FGF9 expression by IHC staining in SCLC tumor sections. Range of FGF9 expression is indicated with intensity scores of 0 (no expression), 1+ (low–moderate expression), and 2+ (high expression). Scale bars, 50 μm. **F,** The frequency of FGF9 intensity scores of SCLC patient tumor samples.

Published OnlineFirst June 3, 2021; DOI: 10.1158/0008-5472.CAN-20-4048

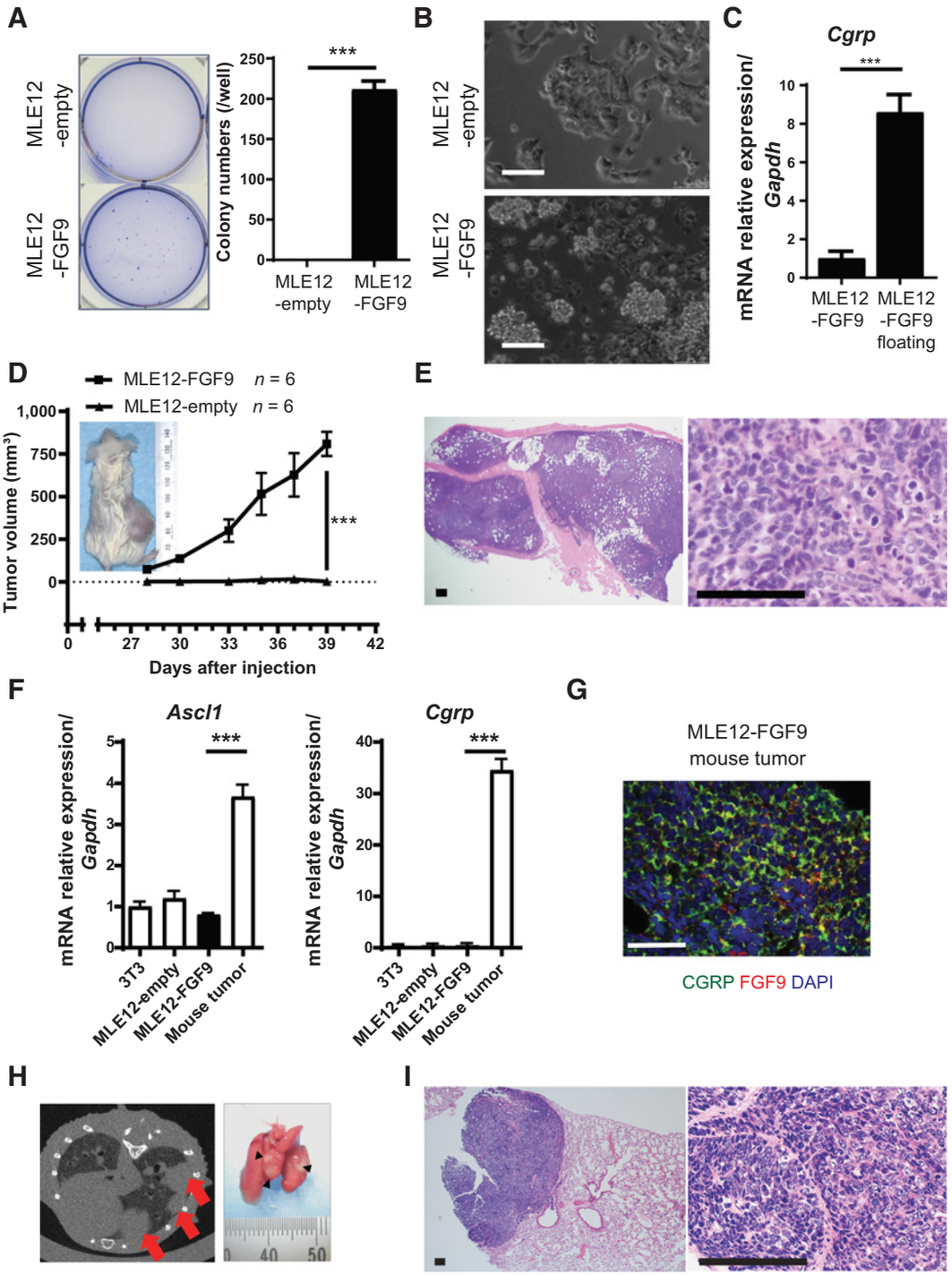

Figure 4.

FGF9-mediated SCLC transdifferentiation in mouse lung adenocarcinoma-derived cells. **A,** Representative images of soft agar colony formation assay for MLE12-empty (vector) and MLE12-FGF9-transduced cells (left). Right, colony number per well ($n = 3$). **B,** Representative images of MLE12-empty and MLE12-FGF9 cells. MLE12-FGF9 cells grew as floating aggregates. Scale bars, 100 μm. **C,** Expression of *Cgrp* in attached versus floating MLE12-FGF9 cells. Error bars, SD. **D,** Representative image of mouse with an MLE12-FGF9 tumor (left), and graph showing tumor volume changes (right). Values indicate average tumor volume in each group ($n = 6$). Error bars, SD. **E,** Representative images of hematoxylin and eosin staining of subcutaneous MLE12-FGF9 tumor sections under low (left) and high (right) power fields. Scale bars, 100 μm. **F,** Expression of *Ascl1* and *Cgrp* relative to the mRNA level of *Gapdh* in NIH-3T3 cells, MLE12-empty (vector) cells, MLE12-FGF9 cells, and MLE12-FGF9 tumors are shown. **G,** Representative images from immunofluorescence analysis of MLE12-FGF9 tumors are shown. FGF9 and CGRP expression is shown. DAPI was used for nuclear staining. Scale bars, 50 μm. **H,** Representative image of a micro-CT of mouse lungs harboring tumors (red arrows; left). Representative image of mouse lungs harboring tumors (right). **I,** Representative images of hematoxylin and eosin staining of MLE12-FGF9 lung tumor sections under low (left) and high (right) power fields. Scale bars, 100 μm. ***, $P < 0.001$.

Published OnlineFirst June 3, 2021; DOI: 10.1158/0008-5472.CAN-20-4048

colony formation *in vitro* (**Fig. 4A**), highlighting the capacity of FGF9 to promote transformation. Interestingly, we found that some MLE12-FGF9 cells detached from the surface of the culture dish and continued to grow as floating aggregates after 3 weeks of culture, which is a characteristic of SCLC cell lines (**Fig. 4B**). These floating cells were collected and examined for expression of *Fgf9* and of several neuroendocrine markers, including *Cgrp*, compared with that in cells that remained attached to the plate. *Cgrp* expression in floating MLE12-FGF9 cells was significantly higher than that in the attached MLE12-FGF9 cells (**Fig. 4C**). These data suggest the possibility that FGF9 functionally contributes to neuroendocrine differentiation.

To confirm the transdifferentiation capacity of FGF9 *in vivo*, mouse allograft model experiments were performed. MLE12-FGF9 or MLE12-empty vector control cells (1.0×10^6) were subcutaneously injected into NOD/SCID mice ($n = 6$/group). Four weeks after injection, all six mice injected with MLE12-FGF9 cells harbored subcutaneous tumors, whereas none of the mice injected with MLE12-empty vector cells had tumors (**Fig. 4D**). Interestingly, the histology of the subcutaneous MLE12-FGF9-derived tumors resembled that of human SCLC, which consists of a pleomorphic population of small, round cells with scanty cytoplasm and hyperchromatic nuclei with homogeneous chromatin dispersion (**Fig. 4E**). Quantitative reverse transcription PCR (qRT-PCR) confirmed increased mRNA levels of the neuroendocrine markers *Ascl1* and *Cgrp* in the formed tumors (**Fig. 4F**). CGRP expression was confirmed at the protein level (**Fig. 4G**). These data are suggestive of FGF9-mediated neuroendocrine differentiation at the molecular level. To rule out potential effects of the subcutaneous tissue microenvironment on epithelial cell differentiation and to confirm that transformation to SCLC can also occur in the lung microenvironment, we injected MLE12-FGF9 cells intravenously *via* the tail vein of NOD/SCID mice. Ten weeks after injection, we confirmed tumor formation in the mouse lungs using μCT (**Fig. 4H**). Again, pathologic analysis revealed histopathologic similarities with human SCLC (**Fig. 4I**). We also transduced a vector encoding the *EGFR* gene harboring the activating L858R mutation or the exon 19 deletion (49), a common lung adenocarcinoma oncogene, into MLE12 cells in order to rule out the possibility of nonspecific SCLC transdifferentiation of MLE12 cells. Transplanting these MLE12-EGFR cells into NOD/SCID mice ($n = 3$, respectively) subcutaneously did not result in tumor formation (Supplementary Fig. S9). These data provide preclinical evidence that FGF9 functionally contributes to SCLC transdifferentiation *in vitro* and *in vivo*.

To elucidate the mechanism underlying FGF9-mediated SCLC transdifferentiation, immunoblotting was performed for MLE12-empty and -FGF9 cells. Increased phosphorylation of ERK but not AKT was observed (**Fig. 5A**), indicating MAPK pathway activation by Fgf9. Recombinant human FGF9 (rhFGF9) also activated the MAPK pathway (**Fig. 5B**). To clarify the corresponding receptors of FGF9-mediated signals, gene knockdown experiments using siRNA was performed. The phosphorylation of ERK was attenuated by *Fgfr1, Fgfr2*, and *Fgfr3* knockdown, indicating that all of these receptors transduce downstream signals; of note, variability was detected partly due to the knockdown efficiency (**Fig. 5C**). Notably, qRT-PCR experiments identified significantly increased mRNA levels of FGF receptors *Fgfr1* and *Fgfr2* (**Fig. 5D**) in MLE12-FGF9 mouse tumors compared with those in MLE12-empty and -FGF9 cells, which suggests FGF9-mediated upregulation of the FGFR pathway in tumors *in vivo*. Immunofluorescence showed the colocalization of FGFR1 and FGF9 or GFP signals in MLE12 tumors (**Fig. 5E**). In addition, to compare the expression levels of *Fgfr* genes between MLE12-FGF9 cells *in vitro* and MLE12-FGF9 cells in the tumors *in vivo*, GFP-positive cells were sorted from the developed tumors. Interestingly, qRT-PCR analysis revealed the clear upregulation of *Fgfr1* and *Fgfr2* in MLE12-FGF9 cells from tumors (Supplementary Fig. S10), suggesting the cell-autonomous expression of FGF receptors. To further confirm that *in vivo* FGF9-mediated transformation occurred through the FGFR pathway and to exclude the contribution of other signaling pathways, we used AZD4547 (50, 51), a pan-FGFR inhibitor, to treat MLE12-FGF9 tumors. Nine NOD/SCID mice were injected subcutaneously with MLE12-FGF9 cells and observed until tumor nodules reached 200 mm^3, at which point, they were treated with either AZD4547 (12.5 mg/kg/day; $n = 5$) or the vehicle ($n = 4$) for 24 days. AZD4547 treatment significantly reduced tumor growth (**Fig. 5F**) compared with vehicle treatment. Collectively, these results indicate that FGF9 induces the transdifferentiation of mouse lung adenocarcinoma-derived cells to SCLC through FGF9-mediated upregulation of the FGFR pathway.

FGF9 induces neuroendocrine differentiation in established human lung adenocarcinoma cells

Next, to confirm the FGF9-mediated neuroendocrine differentiation in established human lung adenocarcinoma-derived cells, we performed further *in vitro* and *in vivo* experiments. To obtain the preclinical evidence for neuroendocrine differentiation in *EGFR*-mutated lung adenocarcinoma cells, we used H1975 cells, which harbor *TP53* and *EGF*R L858R + T790M mutations. We performed a gene knockout of *RB1* using the CRISPR/Cas9 technology in H1975 cells, with or without FGF9 induction (**Fig. 6A**), because inactivation of RB1 is frequently reported in transdifferentiation (28–30). However, no upregulation of the neuroendocrine genes was observed, indicating that TP53 and RB1 inactivation and *FGF9* overexpression were not sufficient to induce neuroendocrine differentiation in H1975 cells. Further, to mimic the clinical situation wherein EGFR-TKI-resistant lung NSCLC transdifferentiates to SCLC, H1975 cells with *RB1* knockout and *FGF9* overexpression were subjected to chronic exposure to osimertinib, which subsequently established osimertinib-resistant (osiR) H1975 cells (**Fig. 6B**). The expression of *ASCL1*, a master regulator of neuroendocrine differentiation, was minimal in the H1975 parental, in the H1975 RB1-knockout, and in the H1975 RB1-knockout with FGF9 transduction cells (**Fig. 6C**). However, *ASCL1* expression was significantly increased in the H1975 RB1-knockout osiR and in the H1975 RB1-knockout osiR with FGF9 transduction cells. These data indicate that inactivation of TP53 and RB1, FGF9 overexpression, and EGFR pathway inhibition are essential to induce neuroendocrine differentiation in H1975 cells. We evaluated two additional *EGFR* mutant lung cancer cell lines, H1650 and BID007 (Supplementary Table S5; Supplementary Figs. S11A and S11B). The inactivation of RB1, overexpression of FGF9, and the inhibition of the EGFR pathway did not induce the upregulation of the neuroendocrine markers in these cells. Thus, it can be inferred that FGF9 induces neuroendocrine differentiation in only a subset of EGFR mutant NSCLC cell lines.

Finally, to examine whether FGF9 expression induces neuroendocrine differentiation in other lung adenocarcinoma cells, we transduced *FGF9* into H2087, H2110, and H2228 lung adenocarcinoma cell lines, which harbor both *TP53* and *RB1* inactivating mutations but not *EGFR*-activating mutations (Supplementary Table S5). We transplanted these *FGF9*-transduced lung adenocarcinoma cells into immunodeficient mice. Although the growth rate of H2087 and H2110 cells was comparable irrespective of FGF9 expression (Supplementary Figs. S12A and S12B), it was significantly higher in *FGF9*-transduced H2228 cells (H2228-FGF9) than in the H2228 cells transduced with an empty

Published OnlineFirst June 3, 2021; DOI: 10.1158/0008-5472.CAN-20-4048

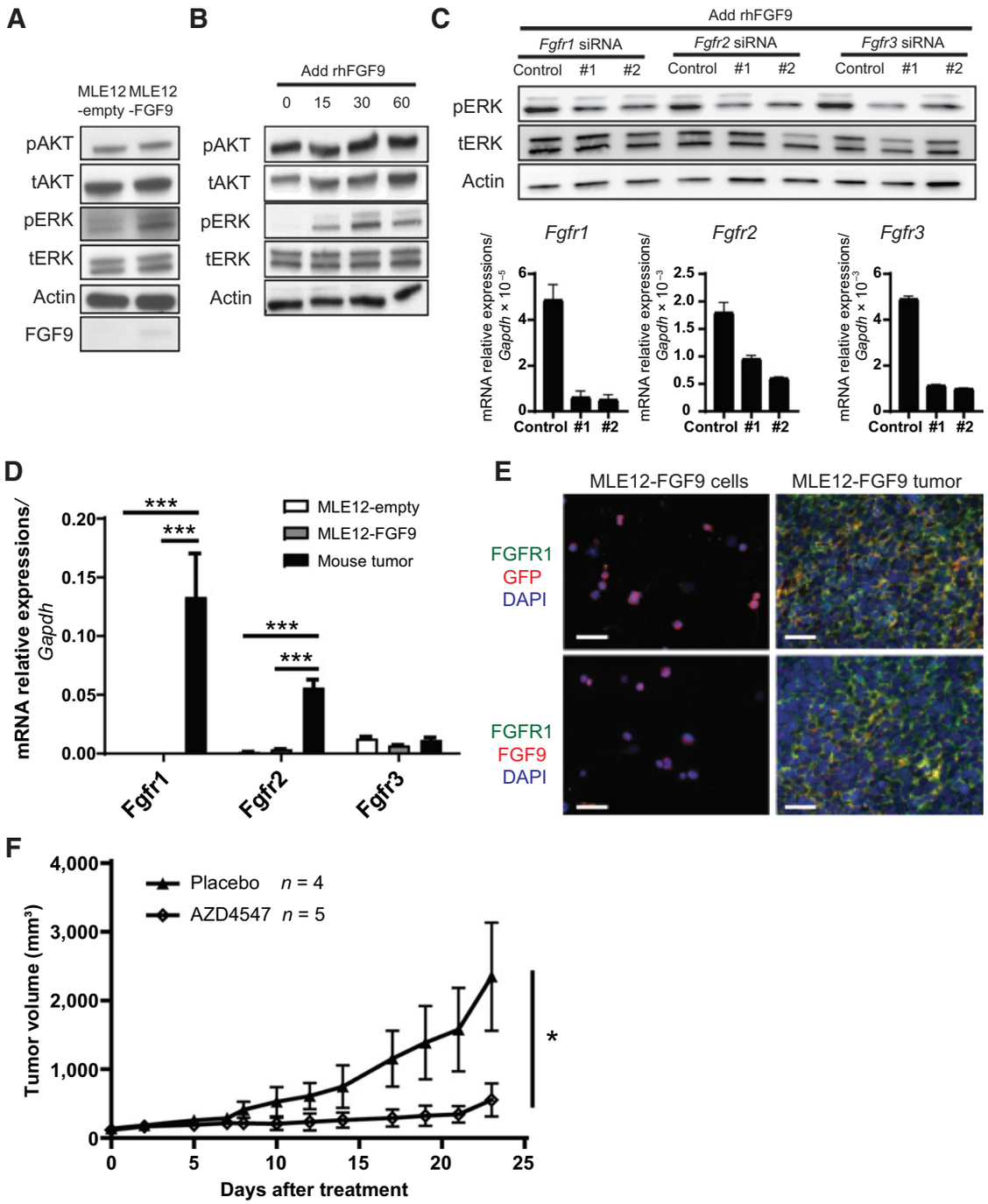

Figure 5.

Contribution of the FGF9–FGFR pathway to the development of MLE12-FGF9-derived SCLC. **A,** Western blot analysis of MLE12-empty (vector) and MLE12-FGF9–transduced cells. **B,** Western blot analysis of MLE12 cells after the addition of rhFGF9 (100 ng/mL). **C,** Western blot analysis of MLE12 cells transfected with siRNA targeting fibroblast growth factor receptor 1 (*Fgfr1*), *Fgfr2*, or *Fgfr3* for 48 hours, followed by the addition of rhFGF9 (top). Phosphorylated (p-) and total (t-) protein forms of the indicated proteins are shown. Actin was used as loading control. The efficiency of *Fgfr* knockdown was confirmed by qRT-PCR (bottom). Error bars, SD. **D,** Expression of *Fgfr1, Fgfr2*, and *Fgfr3* relative to the expression of *Gapdh* for MLE12-empty cells, MLE12-FGF9 cells, and MLE12-FGF9 tumors. ***, $P < 0.001$. Error bars, SD. **E,** Representative images of immunofluorescence analysis of the indicated proteins in MLE12-FGF9 cells and MLE12-FGF9 tumors. DAPI was used for nuclear staining. Scale bars, 100 μm. **F,** Tumor volumes of MLE12-FGF9 tumors with or without AZD4547 treatment. Values indicate average tumor volume in each group; *, $P < 0.05$ for AZD4547 versus vehicle treatment. Error bars, SEM.

Published OnlineFirst June 3, 2021; DOI: 10.1158/0008-5472.CAN-20-4048

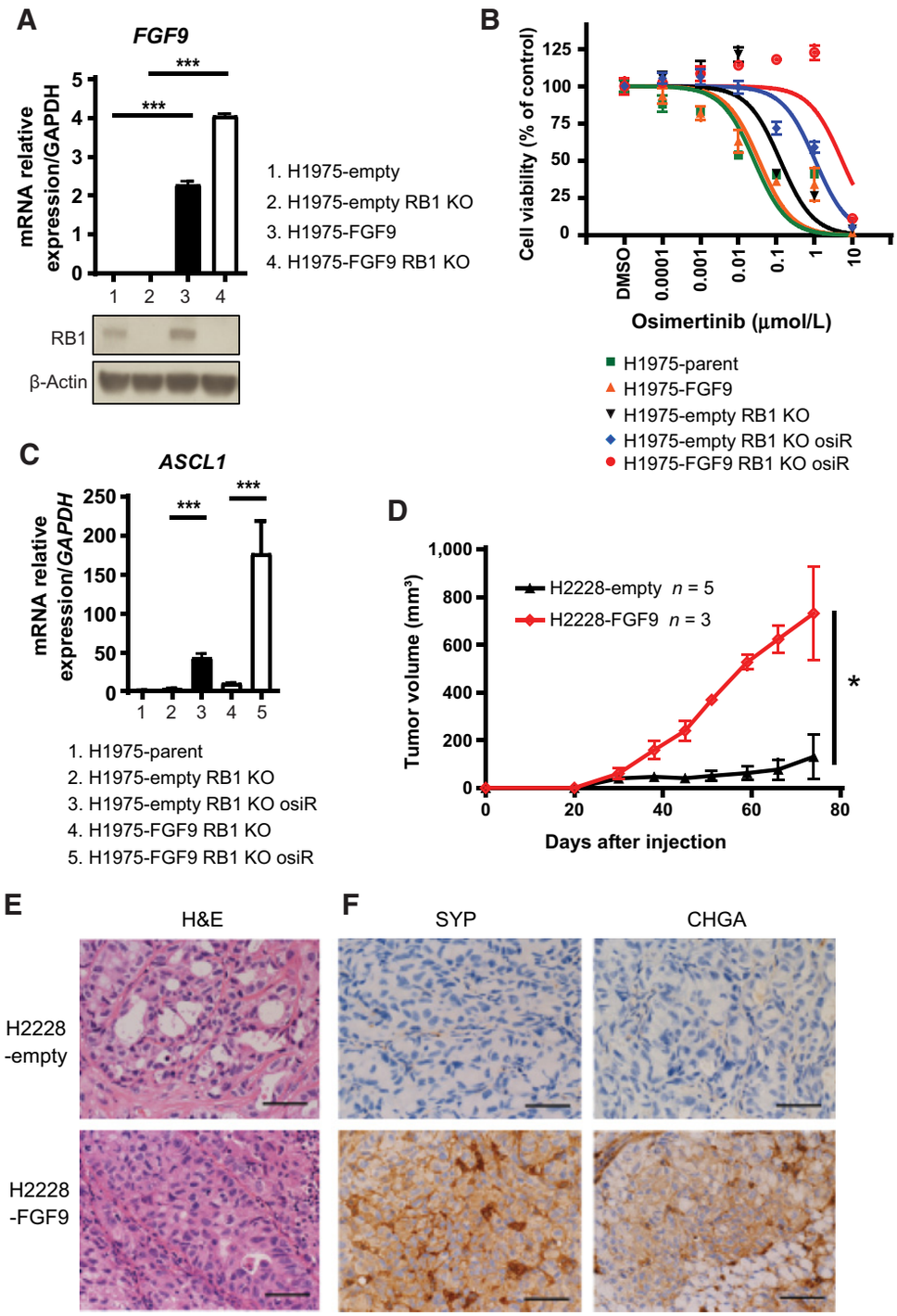

Figure 6.

FGF9 induces neuroendocrine differentiation in established lung cancer cells. **A,** Expression of *FGF9* relative to the expression of *GAPDH* in these cells (top). Western blot analysis of H1975 cells after overexpression of FGF9 and/or knockout of RB1, showing the indicated proteins (bottom). **B,** Relative cell viability of the indicated H1975 cells treated with osimertinib. **C,** Expression of achaete-scute homologue 1 (*ASCL1*) relative to that of *GAPDH* in the indicated H1975 cells. osiR, osimertinib-resistant. **D,** Volumes of xenografted H2228-empty and H2228-FGF9 tumors. Error bars, SD. The values indicate average tumor volume in each group. **E** and **F,** Representative images of hematoxylin and eosin (H&E) staining (**E**) and IHC staining (**F**) for SYP and CHGA in H2228-empty and H2228-FGF9 tumors. Scale bars, 50 μm. *, $P < 0.05$; ***, $P < 0.001$.

Published OnlineFirst June 3, 2021; DOI: 10.1158/0008-5472.CAN-20-4048

vector (H2228-empty; **Fig. 6D**). Histologic analysis revealed that H2087 and H2110 cells formed moderately differentiated adenocarcinoma tumors regardless of FGF9 expression (Supplementary Fig. S12C). In contrast, H2228 cells exhibited histological differences depending on FGF9 expression. Compared with tumors generated from H2228-empty cells, which formed well-differentiated adenocarcinomas, H2228-FGF9 cells formed poorly differentiated adenocarcinomas. The palisading pattern, a characteristic of neuroendocrine differentiation, was observed in H2228-FGF9 tumors but not in H2228-empty tumors (**Fig. 6E**). IHC revealed that the neuroendocrine markers SYP and CHGA were expressed in H2228-FGF9 tumors but not in H2228-empty tumors (**Fig. 6F**), indicating neuroendocrine differentiation in established adenocarcinoma cells. Collectively, the findings provide direct evidence that prospective FGF9 induction functionally contributes to the transdifferentiation of adenocarcinoma to SCLC in established human lung cancer cells.

Discussion

In this study, we identified FGF9 upregulation in lung cancer cases of adenocarcinoma to SCLC transdifferentiation. Although the number of cases evaluated in this study was small ($n = 6$), upregulation of FGF9 was found in 66.7% of patients examined. In addition, aberrant FGF9 expression was observed in a significant proportion of primary SCLC, and it was positively correlated with neuroendocrine marker genes. FGF9 is a developmentally important FGF and its expression is repressed in normal adult lungs. In the pseudoglandular stage of lung development, FGF9 activates signaling pathways to direct epithelial specification and lung branching (52). Recently, the oncogenic roles of FGF9 in multiple cancer types, including lung cancer, have been reported by our research group and other groups (33, 44). However, the role of FGF9 upregulation in primary and transdifferentiated SCLC remain elusive. Although robust upregulation of *FGF9* mRNA was observed, no genetic alterations such as *FGF9* mutations or amplification was identified by WES, indicating that the FGF9 expression level was regulated through epigenetic mechanisms. Recently, long noncoding RNA H19- or microRNA-mediated regulation of the expression of FGF9 has been reported in multiple types of cancers, including SCLC (53–55); in addition, the high expression of H19 was reported in ASCL1 positive cell lines (56). To understand the mechanism of FGF9 upregulation in primary and transdifferentiated SCLC, further epigenetic evaluation such as noncoding RNA, DNA methylation, and chromatin modification studies should be performed.

Interestingly, our cases with transdifferentiation had heavy smoking history, in contrast to the light smoking history of other cohorts (29, 30), and several case reports (14, 15). Tobacco smoking may affect the susceptibility to transdifferentiation. However, to verify the effects of tobacco smoking on transdifferentiation, further clinical evaluations are required.

Transdifferentiation was prospectively demonstrated in multiple mouse and human lung adenocarcinoma-derived cells. To our knowledge, this is the first report that provides direct evidence for transdifferentiation. However, the level of transdifferentiation was variable among cells. In addition, transdifferentiation was not induced in the H2087 and H2110 cells even with TP53 and the RB1 inactivation and FGF9 overexpression. EML4-ALK positive H2228 has transdifferentiated to SCLC, which may explain that transdifferentiation can also occur in ALK-translocated NSCLC after ALK-TKI treatment (10). These findings indicate that specific genetic or epigenetic contexts may affect the level of transdifferentiation. Interestingly, SCLC transdifferentiation was most frequently observed in lung adenocarcinoma with *EGFR*-mutations after long-term EGFR-TKI treatment, when the cancer cells become resistant to EGFR pathway inhibition. Thus, EGFR pathway inhibition may be required for transdifferentiation. In this study, this was supported by the downregulation of *EGFR* mRNA levels in the RNA-seq data of case #1 and the upregulation of the *ASCL1* gene in H1975 osiR cells. The effect of EGFR pathway inhibition in transdifferentiation needs further evaluation.

Clinically, the transdifferentiated patients with SCLC are treated using systemic chemotherapy, including platinum-etoposide or platinum-irinotecan, which is administered in patients with primary SCLC (57). The recent approval of combination therapy with immune-checkpoint inhibitors as first-line treatment for extensive disease SCLC provides another choice of treatment for transdifferentiated patients with SCLC (58, 59). However, the efficacy of immune-checkpoint inhibitors for transdifferentiated SCLC should be further evaluated, because none of 17 patients who received immune-checkpoint inhibitors experienced a response in a retrospective cohort (29). To improve the prognosis of transdifferentiated patients with SCLC, further identification of potential drug targets and the development of a novel therapeutic strategy are needed. The paucity of druggable genetic or epigenetic alterations has hampered the development of molecular targeted therapy in SCLC. Interestingly, we have observed cell-autonomous upregulation of Fgfr1 in transdifferentiated MLE12-FGF9 tumors. Similar cell-autonomous upregulation of Fgfr1 was observed in a genetically engineered mouse lung adenocarcinoma model (60). The upregulation of FGFR1 may be relevant with the finding that amplification of *FGFR1* was observed in approximately 6% of primary SCLC (24). In addition, several studies have suggested the oncogenic roles of FGFR1 in SCLC (23, 61, 62). The upregulation of the FGF9–FGFRs axis may open a new window for the use of FGFR inhibitors in the treatment of transdifferentiated SCLC, as supported by the *in vivo* experiment using AZD4547. To evaluate the efficacy of FGFR inhibitors for the treatment of transdifferentiated SCLC, clinical prospective studies are needed.

In conclusion, we provide preclinical and clinical evidence for FGF9-mediated SCLC transdifferentiation and propose a potential avenue for treatment of transdifferentiated SCLC.

Authors' Disclosures

No disclosures were reported.

Authors' Contributions

Kota Ishioka: Conceptualization, data curation, formal analysis, validation, investigation, visualization, methodology, writing–original draft, writing–review and editing. **Hiroyuki Yasuda:** Conceptualization, data curation, supervision, funding acquisition, writing–original draft, writing–review and editing. **Junko Hamamoto:** Conceptualization, data curation, formal analysis, funding acquisition, validation, investigation, visualization, methodology, writing–original draft, writing–review and editing. **Hideki Terai:** Conceptualization, data curation, formal analysis, funding acquisition, validation, investigation, visualization, methodology, writing–original draft, writing–review and editing. **Katsura Emoto:** Data curation, validation, investigation, visualization, methodology. **Tae-Jung Kim:** Data curation, validation, investigation, visualization, methodology. **Shigemichi Hirose:** Data curation, validation, investigation, visualization, methodology. **Takashi Kamatani:** Investigation. **Sachiyo Mimaki:** Investigation. **Daisuke Arai:** Investigation. **Keiko Ohgino:** Investigation. **Tetsuo Tani:** Investigation. **Keita Masuzawa:** Investigation. **Tadashi Manabe:** Investigation. **Taro Shinozaki:** Investigation. **Akifumi Mitsuishi:** Investigation. **Toshiki Ebisudani:** Investigation. **Takahiro Fukushima:** Investigation. **Mari Ozaki:** Investigation, writing–review and editing. **Shinnosuke Ikemura:** Investigation. **Ichiro Kawada:**

Published OnlineFirst June 3, 2021; DOI: 10.1158/0008-5472.CAN-20-4048

Investigation. **Katsuhiko Naoki:** Investigation. **Morio Nakamura:** Investigation. **Takashi Ohtsuka:** Investigation. **Hisao Asamura:** Validation, investigation. **Katsuya Tsuchihara:** Writing–review and editing. **Yuichiro Hayashi:** Validation, Investigation, visualization, methodology. **Ahmed E. Hegab:** Investigation, writing–review and editing. **Susumu S. Kobayashi:** Investigation, writing–review and editing. **Takashi Kohno:** Investigation, writing–review and editing. **Hideo Watanabe:** Formal analysis, investigation, visualization, methodology. **David M. Ornitz:** Validation, methodology, writing–review and editing. **Tomoko Betsuyaku:** Conceptualization, supervision, funding acquisition, project administration, Writing–review and editing. **Kenzo Soejima:** Conceptualization, supervision, funding acquisition, investigation, project administration, writing–review and editing. **Koichi Fukunaga:** Supervision, validation, project administration, writing–review and editing.

Acknowledgments

This work was supported in part by the Japan Society for the Promotion of Science to K. Soejima (19H03671), T. Betsuyaku (15H04833), H. Terai (18K08184), J. Hamamoto (19K08610), and H. Yasuda (17K09667). This work was also supported in part by the Japan Agency for Medical Research and Development (AMED), grants 20cm0106576 and 20ck0106471 to H. Yasuda, by the Takeda Science Foundation (to H. Terai and H. Yasuda), and by NIH to D.M. Ornitz (HL11119008). We thank Ms. Mikiko Shibuya for her excellent technical assistance. We also thank the Collaborative Research Resources at the Keio University School of Medicine for assistance with cell sorting.

The costs of publication of this article were defrayed in part by the payment of page charges. This article must therefore be hereby marked *advertisement* in accordance with 18 U.S.C. Section 1734 solely to indicate this fact.

Received December 11, 2020; revised April 1, 2021; accepted June 1, 2021; published first June 3, 2021.

References

1. Travis WD, Brambilla E, Nicholson AG, Yatabe Y, Austin JHM, Beasley MB, et al. The 2015 world health organization classification of lung tumors: impact of genetic, clinical and radiologic advances since the 2004 classification. J Thorac Oncol 2015;10:1243–60.
2. Desai TJ, Brownfield DG, Krasnow MA. Alveolar progenitor and stem cells in lung development, renewal and cancer. Nature 2014;507:190–4.
3. Swanton C, Govindan R. Clinical implications of genomic discoveries in lung cancer. N Engl J Med 2016;374:1864–73.
4. Sutherland KD, Proost N, Brouns I, Adriaensen D, Song JY, Berns A. Cell of origin of small cell lung cancer: inactivation of Trp53 and Rb1 in distinct cell types of adult mouse lung. Cancer Cell 2011;19:754–64.
5. Park KS, Liang MC, Raiser DM, Zamponi R, Roach RR, Curtis SJ, et al. Characterization of the cell of origin for small cell lung cancer. Cell Cycle 2011;10:2806–15.
6. Balanis NG, Sheu KM, Esedebe FN, Patel SJ, Smith BA, Park JW, et al. Pan-cancer convergence to a small-cell neuroendocrine phenotype that shares susceptibilities with hematological malignancies. Cancer Cell 2019;36:17–34 e7.
7. Oser MG, Niederst MJ, Sequist LV, Engelman JA. Transformation from non-small-cell lung cancer to small-cell lung cancer: molecular drivers and cells of origin. Lancet Oncol 2015;16:e165–72.
8. Sequist LV, Waltman BA, Dias-Santagata D, Digumarthy S, Turke AB, Fidias P, et al. Genotypic and histological evolution of lung cancers acquiring resistance to EGFR inhibitors. Sci Transl Med 2011;3:75ra26.
9. Yu HA, Arcila ME, Rekhtman N, Sima CS, Zakowski MF, Pao W, et al. Analysis of tumor specimens at the time of acquired resistance to EGFR-TKI therapy in 155 patients with EGFR-mutant lung cancers. Clin Cancer Res 2013;19:2240–7.
10. Takegawa N, Hayashi H, Iizuka N, Takahama T, Ueda H, Tanaka K, et al. Transformation of ALK rearrangement-positive adenocarcinoma to small-cell lung cancer in association with acquired resistance to alectinib. Ann Oncol 2016; 27:953–5.
11. Imakita T, Fujita K, Kanai O, Terashima T, Mio T. Small cell lung cancer transformation during immunotherapy with nivolumab: A case report. Respir Med Case Rep 2017;21:52–5.
12. Ferrer L, Giaj Levra M, Brevet M, Antoine M, Mazieres J, Rossi G, et al. A brief report of transformation from NSCLC to SCLC: molecular and therapeutic characteristics. J Thorac Oncol 2019;14:130–4.
13. Park JW, Lee JK, Sheu KM, Wang L, Balanis NG, Nguyen K, et al. Reprogramming normal human epithelial tissues to a common, lethal neuroendocrine cancer lineage. Science 2018;362:91–5.
14. Morinaga R, Okamoto I, Furuta K, Kawano Y, Sekijima M, Dote K, et al. Sequential occurrence of non-small cell and small cell lung cancer with the same EGFR mutation. Lung Cancer 2007;58:411–3.
15. Zakowski MF, Ladanyi M, Kris MG. Memorial sloan-kettering cancer center lung cancer oncogenome g. egfr mutations in small-cell lung cancers in patients who have never smoked. N Engl J Med 2006;355:213–5.
16. Aggarwal R, Huang J, Alumkal JJ, Zhang L, Feng FY, Thomas GV, et al. Clinical and genomic characterization of treatment-emergent small-cell neuroendocrine prostate cancer: a multi-institutional prospective study. J Clin Oncol 2018;36: 2492–503.
17. Gazdar AF, Bunn PA, Minna JD. Small-cell lung cancer: what we know, what we need to know and the path forward. Nat Rev Cancer 2017;17:765.
18. Bernicker EH, Allen TC, Cagle PT. Update on emerging biomarkers in lung cancer. J Thorac Dis 2019;11:S81–S8.
19. Kris MG, Johnson BE, Berry LD, Kwiatkowski DJ, Iafrate AJ, Wistuba II, et al. Using multiplexed assays of oncogenic drivers in lung cancers to select targeted drugs. JAMA 2014;311:1998–2006.
20. Lu T, Yang X, Huang Y, Zhao M, Li M, Ma K, et al. Trends in the incidence, treatment, and survival of patients with lung cancer in the last four decades. Cancer Manag Res 2019;11:943–53.
21. Borges M, Linnoila RI, van de Velde HJ, Chen H, Nelkin BD, Mabry M, et al. An achaete-scute homologue essential for neuroendocrine differentiation in the lung. Nature 1997;386:852–5.
22. Schaffer BE, Park KS, Yiu G, Conklin JF, Lin C, Burkhart DL, et al. Loss of p130 accelerates tumor development in a mouse model for human small-cell lung carcinoma. Cancer Res 2010;70:3877–83.
23. George J, Lim JS, Jang SJ, Cun Y, Ozretic L, Kong G, et al. Comprehensive genomic profiles of small cell lung cancer. Nature 2015;524:47–53.
24. Peifer M, Fernandez-Cuesta L, Sos ML, George J, Seidel D, Kasper LH, et al. Integrative genome analyses identify key somatic driver mutations of small-cell lung cancer. Nat Genet 2012;44:1104–10.
25. Rudin CM, Durinck S, Stawiski EW, Poirier JT, Modrusan Z, Shames DS, et al. Comprehensive genomic analysis identifies SOX2 as a frequently amplified gene in small-cell lung cancer. Nat Genet 2012;44:1111–6.
26. Ouadah Y, Rojas ER, Riordan DP, Capostagno S, Kuo CS, Krasnow MA. Rare pulmonary neuroendocrine cells are stem cells regulated by Rb, p53, and notch. Cell 2019;179:403–16e23.
27. Semenova EA, Nagel R, Berns A. Origins, genetic landscape, and emerging therapies of small cell lung cancer. Genes Dev 2015;29:1447–62.
28. Niederst MJ, Sequist LV, Poirier JT, Mermel CH, Lockerman EL, Garcia AR, et al. RB loss in resistant EGFR mutant lung adenocarcinomas that transform to small-cell lung cancer. Nat Commun 2015;6:6377.
29. Marcoux N, Gettinger SN, O'Kane G, Arbour KC, Neal JW, Husain H, et al. EGFR-mutant adenocarcinomas that transform to small-cell lung cancer and other neuroendocrine carcinomas: clinical outcomes. J Clin Oncol 2019; 37:278–85.
30. Lee JK, Lee J, Kim S, Kim S, Youk J, Park S, et al. Clonal history and genetic predictors of transformation into small-cell carcinomas from lung adenocarcinomas. J Clin Oncol 2017;35:3065–74.
31. Yasuda H, Park E, Yun CH, Sng NJ, Lucena-Araujo AR, Yeo WL, et al. Structural, biochemical, and clinical characterization of epidermal growth factor receptor (EGFR) exon 20 insertion mutations in lung cancer. Sci Transl Med 2013;5: 216ra177.
32. Wikenheiser KA, Clark JC, Linnoila RI, Stahlman MT, Whitsett JA. Simian virus 40 large T antigen directed by transcriptional elements of the human surfactant protein C gene produces pulmonary adenocarcinomas in transgenic mice. Cancer Res 1992;52:5342–52.
33. Ohgino K, Soejima K, Yasuda H, Hayashi Y, Hamamoto J, Naoki K, et al. Expression of fibroblast growth factor 9 is associated with poor prognosis in patients with resected non-small cell lung cancer. Lung Cancer 2014;83: 90–6.
34. Mascaux C, Wynes MW, Kato Y, Tran C, Asuncion BR, Zhao JM, et al. EGFR protein expression in non-small cell lung cancer predicts response to an EGFR

tyrosine kinase inhibitor–a novel antibody for immunohistochemistry or AQUA technology. Clin Cancer Res 2011;17:7796–807.
35. Theelen WS, Mittempergher L, Willems SM, Bosma AJ, Peters DD, van der Noort V, et al. FGFR1, 2 and 3 protein overexpression and molecular aberrations of FGFR3 in early stage non-small cell lung cancer. J Pathol Clin Res 2016;2: 223–33.
36. Petersen I, Dietel M, Geilenkeuser WJ, Mireskandari M, Weichert W, Steiger K, et al. EGFR immunohistochemistry as biomarker for antibody-based therapy of squamous NSCLC - Experience from the first ring trial of the German Quality Assurance Initiative for Pathology (QuIP (R)). Pathol Res Pract 2017; 213:1530–5.
37. Ghandi M, Huang FW, Jane-Valbuena J, Kryukov GV, Lo CC, McDonald ER 3rd, et al. Next-generation characterization of the cancer cell line encyclopedia. Nature 2019;569:503–8.
38. Chun H, Kim S. BAMixChecker: an automated checkup tool for matched sample pairs in NGS cohort. Bioinformatics 2019;35:4806–8.
39. Alexandrov LB, Kim J, Haradhvala NJ, Huang MN, Tian Ng AW, Wu Y, et al. The repertoire of mutational signatures in human cancer. Nature 2020;578:94–101.
40. Rudin CM, Poirier JT, Byers LA, Dive C, Dowlati A, George J, et al. Molecular subtypes of small cell lung cancer: a synthesis of human and mouse model data. Nat Rev Cancer 2019;19:289–97.
41. He X, Chen SY, Yang Z, Zhang J, Wang W, Liu MY, et al. miR-4317 suppresses non-small cell lung cancer (NSCLC) by targeting fibroblast growth factor 9 (FGF9) and cyclin D2 (CCND2). J Exp Clin Cancer Res 2018;37:230.
42. Yang H, Fang F, Chang R, Yang L. MicroRNA-140–5p suppresses tumor growth and metastasis by targeting transforming growth factor beta receptor 1 and fibroblast growth factor 9 in hepatocellular carcinoma. Hepatology 2013;58:205–17.
43. Mizukami T, Togashi Y, Naruki S, Banno E, Terashima M, de Velasco MA, et al. Significance of FGF9 gene in resistance to anti-EGFR therapies targeting colorectal cancer: A subset of colorectal cancer patients with FGF9 upregulation may be resistant to anti-EGFR therapies. Mol Carcinog 2017;56:106–17.
44. Yin Y, Betsuyaku T, Garbow JR, Miao J, Govindan R, Ornitz DM. Rapid induction of lung adenocarcinoma by fibroblast growth factor 9 signaling through FGF receptor 3. Cancer Res 2013;73:5730–41.
45. Huang Y, Jin C, Hamana T, Liu J, Wang C, An L, et al. Overexpression of FGF9 in prostate epithelial cells augments reactive stroma formation and promotes prostate cancer progression. Int J Biol Sci 2015;11:948–60.
46. Shigematsu H, Lin L, Takahashi T, Nomura M, Suzuki M, Wistuba II, et al. Clinical and biological features associated with epidermal growth factor receptor gene mutations in lung cancers. J Natl Cancer Inst 2005;97:339–46.
47. Colvin JS, White AC, Pratt SJ, Ornitz DM. Lung hypoplasia and neonatal death in Fgf9-null mice identify this gene as an essential regulator of lung mesenchyme. Development 2001;128:2095–106.
48. Wikenheiser KA, Vorbroker DK, Rice WR, Clark JC, Bachurski CJ, Oie HK, et al. Production of immortalized distal respiratory epithelial cell lines from surfactant protein C/simian virus 40 large tumor antigen transgenic mice. Proc Natl Acad Sci U S A 1993;90:11029–33.
49. Paez JG, Janne PA, Lee JC, Tracy S, Greulich H, Gabriel S, et al. EGFR mutations in lung cancer: correlation with clinical response to gefitinib therapy. Science 2004;304:1497–500.
50. Gavine PR, Mooney L, Kilgour E, Thomas AP, Al-Kadhimi K, Beck S, et al. AZD4547: an orally bioavailable, potent, and selective inhibitor of the fibroblast growth factor receptor tyrosine kinase family. Cancer Res 2012; 72:2045–56.
51. Dieci MV, Arnedos M, Andre F, Soria JC. Fibroblast growth factor receptor inhibitors as a cancer treatment: from a biologic rationale to medical perspectives. Cancer Discov 2013;3:264–79.
52. Yin Y, Ornitz DM. FGF9 and FGF10 activate distinct signaling pathways to direct lung epithelial specification and branching. Sci Signal 2020;13.
53. Li X, Lv F, Li F, Du M, Liang Y, Ju S, et al. Long Noncoding RNA H19 facilitates small cell lung cancer tumorigenesis through miR-140–5p/FGF9 axis. Onco Targets Ther 2020;13:3525–34.
54. Wang W, Dong Y, Li X, Pan Y, Du J, Liu D. MicroRNA-431 serves as a tumor inhibitor in breast cancer through targeting FGF9. Oncol Lett 2020;19: 1001–7.
55. Wang Y, Huang Q, Li F. miR-140–5p targeted FGF9 and inhibited the cell growth of laryngeal squamous cell carcinoma. Biochem Cell Biol 2020;98:83–9.
56. Fan B, Pan W, Wang X, Wei M, He A, Zhao A, et al. Long noncoding RNA mediates stroke-induced neurogenesis. Stem Cells 2020;38:973–85.
57. Hanna N, Bunn PA Jr., Langer C, Einhorn L, Guthrie T Jr., Beck T, et al. Randomized phase III trial comparing irinotecan/cisplatin with etoposide/ cisplatin in patients with previously untreated extensive-stage disease small-cell lung cancer. J Clin Oncol 2006;24:2038–43.
58. Horn L, Mansfield AS, Szczesna A, Havel L, Krzakowski M, Hochmair MJ, et al. First-Line Atezolizumab plus Chemotherapy in Extensive-Stage Small-Cell Lung Cancer. N Engl J Med 2018;379:2220–9.
59. Paz-Ares L, Dvorkin M, Chen Y, Reinmuth N, Hotta K, Trukhin D, et al. Durvalumab plus platinum-etoposide versus platinum-etoposide in first-line treatment of extensive-stage small-cell lung cancer (CASPIAN): a randomised, controlled, open-label, phase 3 trial. Lancet 2019;394:1929–39.
60. Arai D, Hegab AE, Soejima K, Kuroda A, Ishioka K, Yasuda H, et al. Characterization of the cell of origin and propagation potential of the fibroblast growth factor 9-induced mouse model of lung adenocarcinoma. J Pathol 2015;235:593–605.
61. Schultheis AM, Bos M, Schmitz K, Wilsberg L, Binot E, Wolf J, et al. Fibroblast growth factor receptor 1 (FGFR1) amplification is a potential therapeutic target in small-cell lung cancer. Mod Pathol 2014;27:214–21.
62. Ferone G, Song JY, Krijgsman O, van der Vliet J, Cozijnsen M, Semenova EA, et al. FGFR1 oncogenic activation reveals an alternative cell of origin of SCLC in Rb1/p53 Mice. Cell Rep 2020;30:3837–50 e3.

Cancer Research
The Journal of Cancer Research (1916–1930) | The American Journal of Cancer (1931–1940)

AACR American Association for Cancer Research

Upregulation of FGF9 in Lung Adenocarcinoma Transdifferentiation to Small Cell Lung Cancer

Kota Ishioka, Hiroyuki Yasuda, Junko Hamamoto, et al.

Cancer Res 2021;81:3916-3929. Published OnlineFirst June 3, 2021.